Random Cluster Number Feature and Cluster Characteristics of Indoor Measurement at 28 GHz

Chao Wang, *Student Member, IEEE*, Jianhua Zhang, *Senior Member, IEEE*, and Fredrik Tufvesson, *Fellow, IEEE*

***Abstract*—In this letter, we analyze cluster characteristics and millimeter wave channel characteristics based on an indoor channel measurement campaign at 28 GHz. The spatial properties of clusters are analyzed, and we investigate the intra-cluster angular spreads and the number of clusters. Also, we introduce the random cluster number (RCN) feature to the primary module of the International Mobile Telecommunications (IMT)-2020 channel model. The RCN is based on a Poisson distribution to simulate the evolution of clusters above 6 GHz to get distributions closer to real channel conditions. Examples of the singular value distributions with and without the RCN feature are given. From the comparisons, we can see the benefits of using the RCN feature in simulations with the IMT-2020 model.**

***Index Terms*—Channel model, International Mobile Telecommunications (IMT)-2020, millimeter (mm) wave measurement, Poisson distribution, random cluster.**

I. Introduction

A CLUSTER is defined as a group of multipath components (MPCs) with similar parameters, e.g., the angle of arrival, the angle of departure, and delay. This concept reduces the computational complexity in data processing, provides a basis for geometry-based stochastic channel models, and helps us to understand the channel behavior.

For the number of clusters, the primary module of an International Telecommunications Union – Radiocommunication Sector (ITU-R) follows the large-scale parameters of a 3rd Generation Partnership Project Technical Report (3GPP TR) 38.900. It specifies a fixed number based on the specific environment, and this is also equal to the corresponding number below 6 GHz. This implies that the multipath richness and sparsity structure in millimeter (mm) wave bands are modeled in the same way as in the micro wave bands, though many papers show that mm wave bands have a more sparse scattering structure [1], [2]. In [3], the average number of clusters is 3.52 and 4.58 for in-building and urban scenarios, respectively, in 28 GHz non line-of-sight (NLoS) channels, with a distribution described by a positive Poisson distribution. Wu *et al.* [4] investigate the intra-cluster characteristics of 28 GHz NLoS channels in an urban micro scenario and show that the mean number of clusters in the measurement is 3.4. These numbers are obviously smaller than those reported in the above-mentioned 3GPP standard and the primary module of the International Mobile Telecommunications (IMT)-2020 model.

Considering this, we performed an indoor measurement campaign at 28 GHz under both line-of-sight (LoS) and NLoS conditions to analyze the delay–azimuth angle of arrival (AAoA) and power-AAoA profiles of clusters and their number. The random cluster number (RCN) is introduced to complement the primary module of the IMT-2020 channel model. It uses a Poisson distribution to simulate the evolution of the number of clusters and modifies the scaling factors for the AAoA, the azimuth angle of departure (AAoD), the elevation angle of arrival, and the elevation angle of departure generation.

This letter contributes to the improvement of the modeling of the cluster characteristics in mm wave indoor scenarios and shows a more realistic solution to generate the number of clusters in the IMT-2020 channel model, which is now accepted in Section 5.9 of ITU-R M. 2412. The remaining part of this letter is organized as follows: Section II describes the measurement details and data processing methods. Section III gives numerical results, including the spatial distributions of clusters, the intra-cluster azimuth angular spreads of arrival (AASA), and the number of clusters, which are calculated for the validation of the primary module of the IMT-2020 channel model. The RCN feature is introduced in Section IV, and we also present channel simulations to show the differences in channel singular values. Finally, the conclusions are drawn in Section V.

II. Measurement and Data Processing

The channel measurements are performed in an indoor hall using a broadband correlator channel sounder with 400 MHz bandwidth at 28 GHz. A virtual array setup is used to form an omnidirectional antenna array in azimuth at the receiver (Rx) side.

Manuscript received July 16, 2018; revised August 25, 2018; accepted August 26, 2018. Date of publication September 5, 2018; date of current version October 4, 2018. This work was supported in part by the National Science and Technology Major Project of the Ministry of Science and Technology under Grant 2017ZX03001012-003, in part by The Ministry of Education China Mobile Research Fund under Grant MCM20160105, in part by the National Natural Science Foundation of China under Grant 61322110, and in part by the Exploratory Project of the State Key Laboratory of Networking and Switching Technology under Grant NST20170205. *(Corresponding author: Jianhua Zhang.)*

C. Wang is with the Key Laboratory of Universal Wireless Communications, Ministry of Education, Wireless Technology Innovation Institute, Beijing University of Posts and Telecommunications, Beijing 100876, China (e-mail: chaowang@bupt.edu.cn).

J. Zhang is with the State Key Laboratory of Networking and Switching Technology, Beijing University of Posts and Telecommunications, Beijing 100876, China (e-mail: jhzhang@bupt.edu.cn).

F. Tufvesson is with the Department of Electrical and Information Technology, Lund University, Lund SE-221 00, Sweden (e-mail: fredrik.tufvesson@eit.lth.se).

Digital Object Identifier 10.1109/LAWP.2018.2868808

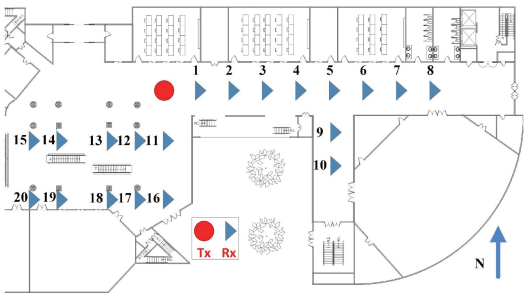

Fig. 1. Measurement map, pos 1–8, 11, and 16 have LoS conditions, pos 9, 10, and 17–20 have NLoS conditions, and pos 12–15 have OLoS conditions.

The measurements were carried out at the ground floor of Teaching Building no. 3, Beijing University of Posts and Telecommunications (see Fig. 1), which can be seen as a typical indoor hotspot (InH) scenario. A sector antenna is used with a 90° half-power beamwidth (HPBW) in azimuth at the transmitter (Tx) side. Its direction is always set towards the position of the Rx. At the Rx side, a rotational high-gain horn antenna with a 10° HPBW in azimuth is used. The channel is measured in 20 different Rx positions; positions (pos) 1–8, 11, and 16 have LoS conditions, pos 9, 10, and 17–20 have NLoS conditions, while pos 12–15 have obstructed LoS (OLoS) conditions. Blocking objects are mainly concrete walls, pillars, stairs, and windows. Using the virtual array measurement method proposed in [5], the horn is rotated in steps of 5° for 72 times to form a virtual omnidirectional antenna array in azimuth. For each Rx position, the initial direction of the horn is east, and it is rotated in the anticlockwise direction.

After collecting the raw data, we combine the 72 channel impulse responses (CIRs) into one group. The CIR of the ith angle bin can be described as follows:

$$h_i(t,\tau) = \sum_{n=1}^{N} \alpha_n^{(i)} e^{-j\phi_n^{(i)}}(t)\delta(\tau - \tau_n^{(i)}) \tag{1}$$

where $i = 1, 2, \ldots, 72$.

$\alpha_n^{(i)}$, $\phi_n^{(i)}(t)$, and $\tau_n^{(i)}$ represent the amplitude, phase, and delay of the nth sample in the time domain at the ith angle bin, respectively. N is the number of collected CIRs.

Then, the CIRs are combined into a group as follows:

$$h_{\text{virtual}}(t,\tau) = [h_1(t,\tau), h_2(t,\tau), \ldots, h_{72}(t,\tau)] \tag{2}$$

where $h_{\text{virtual}}(t,\tau)$ can be considered as the equivalent CIR collected from an omnidirectional antenna array in azimuth. It is noted that, in the measurements, three times oversampling of the CIRs is used, the length of the pseudo-noise (PN) sequences is 1553, and each time, 400 snapshots are collected. In each direction, we spend $[1/(400 \times 10^6 \times 3)] \times 1553 \times 400 = 511$ μs to collect the data. For all the directions, the measurement time will be much longer; the channel is assumed to be static, and the combined CIR can only be seen as an equivalent CIR under static conditions.

The MPCs are estimated by the space-alternating generalized expectation maximization algorithm, thereby giving a joint estimate of the parameter set $\{\tau_l, f_{d,l}, \Phi_l, \Omega_l, \alpha_l\}$. τ_l, $f_{d,l}$, Φ_l, Ω_l, and α_l denote the propagation delay, the Doppler shift, the AoD, the AoA, and the polarization of the lth propagation MPC, respectively.

The number of estimated MPCs is set to 100 in each snapshot. In this letter, only angles at the Rx side are estimated and used for further analysis. In the final step, we cluster the MPCs by using the *K*-power-means clustering algorithm to group MPCs with similar properties so as to study the cluster behavior. It is noted that if the measurement is performed on dynamic channels, real-time measurements and cluster tracking are preferred [6]–[8].

III. Numerical Results

A. Spatial Distribution of Clusters

In Fig. 2, we plot examples of delay–AAoA profiles of MPCs and clusters in Cartesian coordinates under LoS, OLoS, and NLoS conditions. Each red square in the figure represents the position of an MPC, while a blue circle represents the position of a cluster. The size of each square/circle represents the power of the corresponding MPC/cluster in dB.

Under the LoS conditions of pos 3, more than 99% of the power comes from the main path near 180° with a delay of 50.2 ns. The remaining power appears near 0° with a delay of 162.0 ns, which is probably due to reflections. At pos 11, under OLoS conditions, the relative power of the main path becomes 44.2%, while under NLoS conditions, the strongest cluster appears at 46.6° with a delay of 86.5 ns, having 75.1% of power at pos 10, whereas the strongest cluster has 41.9% of power at 72.6° with a delay of 65.6 ns for pos 17.

B. Intra-Cluster Angular Spread of Arrival and the Number of Clusters

The intra-cluster angular spread is also dependent on the propagation conditions and receiver position. It is calculated as follows:

$$\sigma_{\text{AS},k} = \sqrt{\sum_{l=1}^{L_k} (\varphi_{l,k} - \mu_k)^2 \cdot P_{l,k} \Big/ \sum_{l=1}^{L_k} P_{l,k}} \tag{3}$$

where $\varphi_{l,k}$ denotes the angle of the lth MPC of the kth cluster, L_k is the number of MPCs of the kth cluster, $P_{l,k}$ is the power of the lth MPC of the kth cluster, and μ_k is the center angle of the kth cluster, which is given by

$$\mu_k = \left(\sum_{l=1}^{L_k}\right) \varphi_{l,k} \cdot P_{l,k} \Big/ \left(\sum_{l=1}^{L_k} P_{l,k}\right). \tag{4}$$

As presented in Table I, the LoS channels have the largest mean value of the AASA; they follow a Gaussian distribution with a mean of 8.1° and a standard deviation of 5.3°, $N(8.1, 5.3)$. Under NLoS conditions, they follow $N(6.8, 6.0)$. Comparing with the standard model, under LoS conditions, the mean is 8°, while it is 11° under NLoS conditions.

The comparison of the number of clusters between measurements and the primary module of the IMT-2020 is also given in Table I. Obviously, it is neither close to 15 under LoS conditions nor 19 under NLoS conditions, as in the case presented in [9].

IV. New Feature in IMT-2020: RCN

Different standards and papers give different views of the number of clusters in a certain environment. The NYUSIM model [10] defines time clusters and spatial lobes. The former

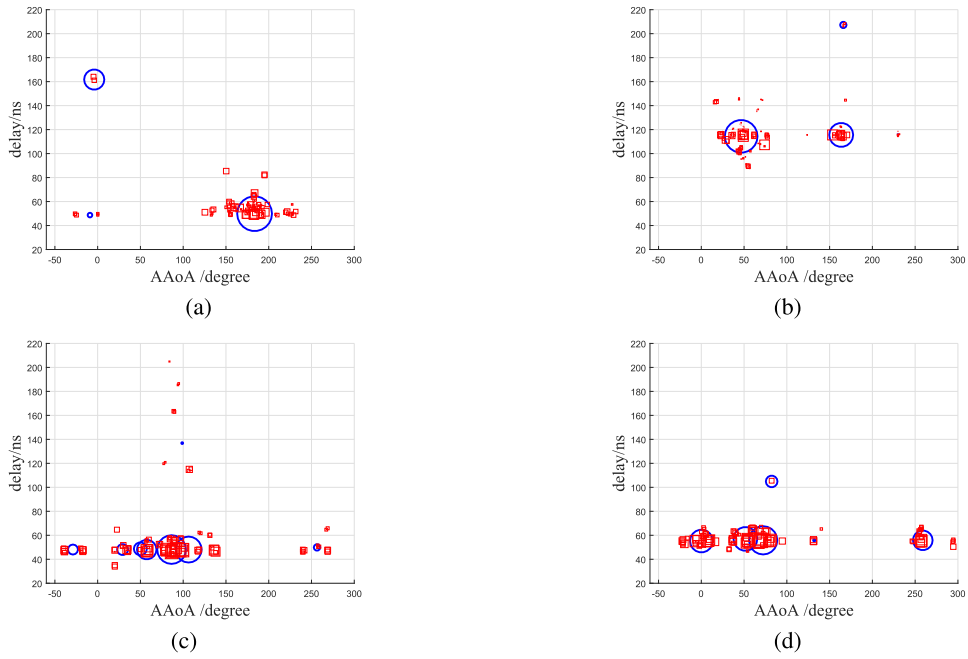

Fig. 2. Four examples of the delay–AAoA profiles of clusters (90° faces the north direction) in Cartesian coordinates. Each blue circle represents the position of a cluster, while each red square represents the position of an MPC. The size shows its power in dB. (a) pos 3 (LoS). (b) pos 10 (NLoS). (c) pos 11 (OLoS). (d) pos 17 (NLoS).

TABLE I
ANGULAR SPREAD OF ARRIVAL (°) AND THE NUMBER OF CLUSTERS IN THE MEASUREMENT

		LoS	NLoS
AASA	5th percentile	0.6	0.0
	50th percentile	7.7	6.9
	95th percentile	15.9	21.5
	Normal Distribution	(8.1, 5.3)	(6.8, 6.0)
AASA in primary module of IMT2020 [8]		8	11
Mean Number of Clusters		4.4	5.7

one is a group of subpaths traveling closely in time space, and the latter one is defined as a departing or incoming direction of power in azimuth and/or elevation. The models of the WINNER family assign one cluster with one angular direction and generate small-scale parameters of clusters based on the measured statistical distributions. COST 2100 defines a concept called visibility regions that can model the evolution of the clusters during movements [11]. Once a terminal moves into the visibility region, the corresponding clusters are active. This method gives a smooth transition of clusters in a mobile scenario. In the 3GPP TR 38.900 [12] and TR 38.901 [13], tables of large-scale parameters defining all the reference parameters of a channel are given, wherein the number of clusters are fixed in different scenarios, e.g., 20 in the urban micro (UMi) scenario. The primary module of the ITU-R IMT-2020 channel model follows the large-scale parameters listed in TR 38.900, above 6 GHz [9]. However, the sparser scattering structure of the mm wave channel makes the use of many statistical distributions to model the performance of multiple input multiple output (MIMO) below 6 GHz unsuitable.

Considering this and the above-mentioned measurement results, we propose to modify the number of clusters in the standard. To implement the RCN feature, we suggest some modifications of the small-scale parameter generation from step

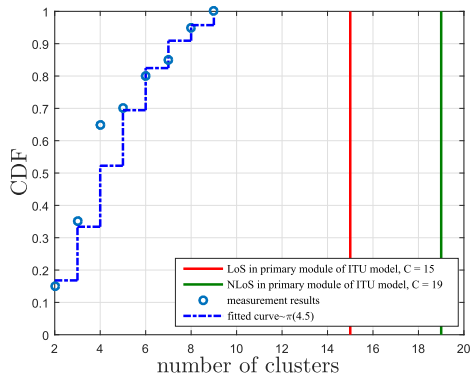

Fig. 3. CDFs of the number of clusters in the measurements, Poisson-based simulation, and listed in the primary module of the IMT-2020 model.

5 in the primary module. Before generating the cluster delay, power, and angles in azimuth and elevation, the number of clusters has to be determined.

For the intensity of clusters, a Poisson distribution is used with intensity λ, which is also the mean value of the random number. Typical values for λ are in the range of 3–10. After generating the number of clusters, the scaling factors for angular spreads have to be updated (see Table A1-33, A1-34 and A1-35 in [9]) so that the angles of the clusters in azimuth and/or elevation can be generated. It is to be noted that the number of clusters has to be generated for each simulation drop. Fig. 3 shows the number of clusters in the measurements, Poisson-based simulation, and the primary module in the IMT-2020 model. Obviously, the fitted curve is close to the measurement results. Hence, we believe that, with the RCN feature, the channel simulations will get closer to real channel conditions.

Fig. 4 shows the cumulative distribution function (CDF) of the largest four singular values and the singular value spread

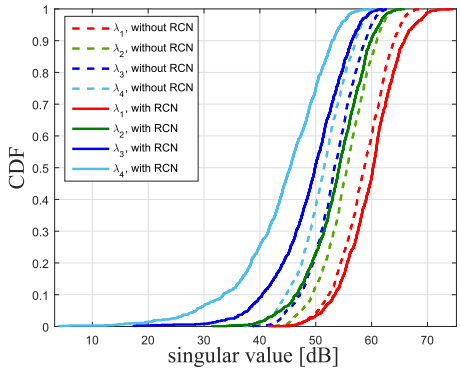

(a)

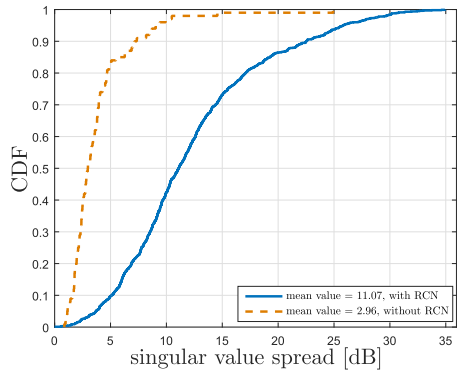

(b)

Fig. 4. Comparisons of singular value distributions using the IMT-2020 channel model with and without the RCN feature. (a) Largest four singular values. (b) Singular value spread.

simulated by the IMT-2020 channel model with and without the RCN feature. Usually, singular values are used to analyze the orthogonality between antennas or between users. In this letter, singular value distributions are used as the indicators to show the differences in orthogonality with and without the RCN feature. A single-cell MIMO system is assumed at 28 GHz with 100 MHz bandwidth in InH scenario. At the Tx side, a uniform linear array (ULA) with 64 cross-polarized antennas is used; at the Rx side, an 8-antenna ULA is used. The channel realizations in the simulation are based on 1000 drops.

As shown in Fig. 4, the singular value spread is different between the simulations with and without the feature. The singular value spread is calculated as [14] follows:

$$\kappa_i = \frac{\max\{\delta_i\}}{\min\{\delta i\}} \tag{5}$$

where δ_i is the singular value of the ith drop. We can see that the differences between singular value distributions become larger for the weaker singular values shown in Fig. 4(a). In Fig. 4(b), the mean singular value spread is 11.1, while it is only 3.0 without the RCN. This is due to the richer scattering in the model without the RCN feature. Fig. 3 shows that the number of clusters in simulations with the RCN feature is closer to realistic cases. Given this, we believe that simulations with the RCN feature are more realistic.

V. Conclusion

In this letter, an indoor measurement campaign at 28 GHz is described and analyzed. The delay–AAoA profiles of clusters and intra-cluster AASA are shown. The number of clusters is calculated to be 4.4 under LoS conditions, while it is found to be 5.7 under NLoS conditions, which are much smaller than the corresponding values in the primary module of the IMT-2020 channel model. Considering this, the RCN feature is proposed to generate the number of clusters in the simulations. The intensity λ of the Poisson distribution is given based on the measurements ($\lambda = 4.5$). We compare the results of singular values between the channel model with and without the RCN feature by simulations. It is shown that the simulations with the RCN feature give larger singular spreads and result in more realistic channel simulations.

Acknowledgment

The authors thank Z. Wu, T. Jiang, and M. Shafi for several discussions. The support provided by the China Scholarship Council during a visit of C. Wang to Lund University is acknowledged (File no. 201706470023).

References

[1] O. E. Ayach, S. Rajagopal, S. Abu-Surra, Z. Pi, and R. W. Heath, "Spatially sparse precoding in millimeter wave MIMO systems," *IEEE Trans. Wireless Commun.*, vol. 13, no. 3, pp. 1499–1513, Mar. 2014.

[2] T. S. Rappaport *et al.*, "Millimeter wave mobile communications for 5G cellular: It will work!," *IEEE Access*, vol. 1, pp. 335–349, May 2013.

[3] J. Ko *et al.*, "Millimeter-wave channel measurements and analysis for statistical spatial channel model in in-building and urban environments at 28 GHz," *IEEE Trans. Wireless Commun.*, vol. 16, no. 9, pp. 5853–5868, Sep. 2017.

[4] S. Wu, S. Hur, K. Whang, and M. Nekovee, "Intra-cluster characteristics of 28 GHz wireless channel in urban micro street canyon," in *Proc. IEEE Global Commun. Conf.*, Dec. 2016, pp. 1–6.

[5] Z. Hu, L. Tian, P. Tang, T. Jiang, and J. Zhang, "The effects of the rotating step on analyzing the virtual multi-antenna measurement results at 28 GHz," in *Proc. IEEE 86th Veh. Technol. Conf.*, Sep. 2017, pp. 1–5.

[6] C. Huang, R. He, Z. Zhong, Y. Geng, Q. Li, and Z. Zhong, "A novel tracking-based multipath component clustering algorithm," *IEEE Antennas Wireless Propag. Lett.*, vol. 16, pp. 2679–2683, 2017.

[7] N. Czink, C. Mecklenbrauker, and G. del Galdo, "A novel automatic cluster tracking algorithm," in *Proc. IEEE 17th Int. Symp. Pers., Indoor Mobile Radio Commun.*, Sep. 2006, pp. 1–5.

[8] J. Zhang, "The interdisciplinary research of big data and wireless channel: A cluster-nuclei based channel model," *China Commun.*, vol. 13, pp. 14–26, 2016.

[9] ITU-R, "Guidelines for evaluation of radio interface technologies for IMT-2020," Geneva, Switzerland, Rep. ITU-R M.2412, 2017.

[10] T. S. Rappaport, S. Sun, and M. Shafi, "Investigation and comparison of 3GPP and NYUSIM channel models for 5G wireless communications," in *Proc. IEEE 86th Veh. Technol. Conf.*, Sep. 2017, pp. 1–5.

[11] L. Liu *et al.*, "The COST 2100 MIMO channel model," *IEEE Wireless Commun.*, vol. 19, no. 6, pp. 92–99, Dec. 2012.

[12] 3GPP, "Study on channel model for frequency spectrum above 6 GHz (version 15)," 3rd Generation Partnership Project (3GPP), Tech. Rep. [Online]. Available: http://www.3gpp.org/ftp/specs/archive/38_series/38.900/. Accessed: Jun. 29, 2018.

[13] 3GPP, "Study on channel model for frequency from 0.5 to 100 GHz (version 14.3.0)," Tech. Rep. [Online]. Available: https://portal.3gpp.org/desktopmodules/Specifications/SpecificationDetails.aspx?specificationId=3173. Accessed: Jan. 5, 2018.

[14] X. Gao, O. Edfors, F. Rusek, and F. Tufvesson, "Massive MIMO performance evaluation based on measured propagation data," *IEEE Trans. Wireless Commun.*, vol. 14, no. 7, pp. 3899–3911, Jul. 2015.